Escola de Camins
Escola Tècnica Superior d'Enginyeria de Camins, Canals i Ports
UPC BARCELONATECH

TREBALL FINAL DE GRAU

Numerical model for material parameter identification of cells

Treball realitzat per:
Juan Pedro Roldán Blasco

Dirigit per:
Jose Javier Muñoz Romero, Vito Conte

Grau en:
Enginyeria Civil

Barcelona, 27 Gener 2017

Departament de Matemàtica Aplicada III

Contents

January 27, 2017

Acknowledgements

I would like to thank, in first place, my supervisors Vito Conte and Jose Javier Muñoz. Vito Conte is the group leader of the Mechanics of development and disease at Institute for Bioengineering of Catalonia (IBEC). His guidance and experience on cell mechanics and research, as well as his infinite patience and advice during hard times have proven to be invaluable to me. Jose Javier Muñoz is an associate professor at UPC, as well as a researcher on biophysics, biomechanics and numerical modelling. His insight on FEM mechanics and non-linear elasticity have been like a lighthouse for a lost ship. Vito and Jose have been always ready to answer any doubt I could have and to teach me the insights of research, even when I did not follow their lines. I am really grateful for having them as supervisors.

I would like to thank, in second place, my former colleague Santi Sempere, who continued the project presented here and helped me the last months of work and I am very thankful to him for that.

I would also like to thank my friend Estemishe and my brother Antonio. They were always there, and they have been the best supporters I have ever had.

Finally, I must express my infinite gratitude to my older siblings and my mother. Without them, this thesis would not have been finished on time.

Juan Pedro Roldán Blasco.

Introduction

An increasing amount of experimental evidence is showing that changes in the mechanical properties of cells are associated to disease progression [1-6], with cancer being among the most impacting on patients. In order to measure these cellular physical changes, several experimental methods have been developed that couple in vitro biomechanical assays, continuum mechanics theory and computational protocols. One of these methods has been developed by Le Berre et al. [8] and consists in a devise for the soft confinement and deformation of cells in vitro. In this work, we will build a computational physical model of the soft confiner, which further allows to quantify the degree of elasticity in the compliance that cells experimentally present to deformation. We carried out this effort in collaboration with scientists at the Institute of Bioengineering of Catalonia (IBEC) and at the University College London (UCL), who provided the experimental basis of the model. The *in silico* physical model we have developed is founded on a set of working assumptions that, on the one hand, aims at simplifying the complexity of cellular biomechanics and, on the other hand, aims at providing experimentalists with a handy computational tool for the an efficient assessment of cell stiffness in vitro. In chapter 1 we briefly describe the biological context of my work and the goal of the project. In chapter 2, we present the *in silico* model of the soft confiner. In chapter 3 we present the results of our studies. In chapter 4 we discuss our results along with future works.

1 Biological background

1.1 Biology overview

Eukaryote cells are composed of an external membrane and a cytoplasm with the different organelles such as nucleus, mitochondria or ribosomes [1]. Although their interaction is complex, we can divide cells' elements in two groups, taking into account their role in cell response to deformation. External wall and cytoskeleton are those responsible for the cell's response to deformation, and the cytoplasm with the rest of the organelles are the determinants of the cell's shape[1,4].

Cellular membranes are mostly made of protein and lipid layers that work as a wall between the cell's interior and the external world [1]. The cytoskeleton is a network of filaments that extends throughout the whole cell. It branches to the inner face of the cell's wall, forming a layer called actin cortex. The coupling between the cell membrane, the actin cortex and the cell interior is considered to give rise to the characteristic visco-elastic response to deformation that has been experimentally observed [1-4].

1.2 Biomechanical assays

Biomechanical assays are experimental setups for the study of mechanical properties of cells and tissues. These setups provide experimental datasets that often consist of measurements of cell deformation. These datasets constitute the experimental basis for theoretical or computational models that are coupled to the experimental set-ups to allow further quantification of mechanical properties of cells. Among these set-ups, it is worth mentioning:

- **Atomic Force Microscopy :** This is the most popular assay. Cells are deformed by their contact interaction with the free end of microscopic cantilever. Registering the deflection of the cantilever and the deformation of the cell, the applied force and then the stiffness of the cell are [1]. As the contact is performed on a small portion of the cell's surface, the non-homogeneity of cellular structure plays an important role. Moreover, the viscous nature of the cells mean that the rate at which the load is applied is also a factor that has to be taken into account. To avoid this phenomenon, some analysis are limited to the range of small deformations, coupling linear elastic models to obtain apparent stiffness values.

- **Optical stretcher :** In this approach, a double laser beam is passed through a suspended cell, stretching it in opposite directions [3,7]. The applied force is then calculated through laser physics, using the change of properties the laser experiences. Two linear elastic models of the cell (either as an elastic sphere or as an elastic shell) have been used to retrieve the elastic moduli of the cells after analysing the forces and the registered deformation [7].

- **Mechanical micro-plate stretcher :** This procedure stretches cells several times with a known load. The observed deformations are introduced into a spring model to retrieve the stiffness of the cell [11].
- **Laser ablation:** This method is used in the study of cell's cortex. Laser rays are used to cut the cortex surface. Monitoring the effects of said cuts, physical parameters such as the propagation of the stress or the time of stress relaxation are calculated. These parameters are then used to define the visco-elastic behaviour of the material [10].

1.3 Dynamic cell confinement

The previously presented assays have to choose between cell confinement control and the number of tested cells [7]. Classic methods like Atomic Force Microscopy work one cell at a time, and those allowing the study of large groups of cells (like the Optical Stretcher presented in [7]) are limited in their confinement capabilities. For our approach, we obtain data through a novel biomechanical assay called dynamic cell confiner, developed by M. le Berre et al [8].

1.3.1 Elastic confinement

The dynamic cell confinement is a non-destructive method consisting in putting a group of scattered isolated cells under an environment of controlled stiffness and geometry. Cells are confined between the glass slide they are cultured and one gel slide of known stiffness. The glass slide can be functionalised in order to either keep cells in suspension over it or to allow them to adhere to it. This adhesion determines the shape adopted by the cell, which is spherical for suspended cells and semi-spherical or dome-shaped for attached cells. A schematic of the experimental set-up is illustrated in figure 1.

The machine has an empty chamber covered by a elastic membrane with a piston and the gel slide attached to it. After applying vacuum in the chamber, the membrane is deformed due to the difference between internal pressure and atmospheric pressure. This moves the piston downwards, pressing the gel over the cell culture. Modifying the chamber pressure, the piston position and the pressure applied over the gel can be regulated.

Once the cells are surrounded by the gel, their deformation can be easily observed using common optical techniques. Then, knowing the gel stiffness, the pressure applied and the deformation the cells experience, the next step will be to relate this data with the physical parameters of the studied cells using a computational physical model.

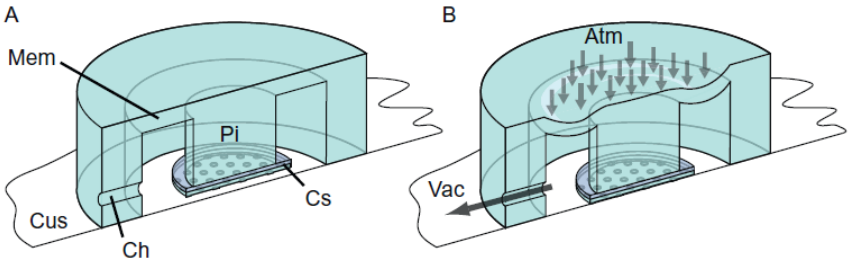

Figure 1: Dynamic confiner scheme, adapted from M. le Berre et al [8]. The left image, state A, shows the confiner before to vacuum. We can see the Piston (Pi) with the attached confiner slide (Cs) over the cell culture substrate (Cus). In state B, vacuum is created through channel (Ch), causing the membrane (Mem) to go down together with the piston and the confinement slide

2 Numerical model

This section provides the development of the FEM used to simulate the dynamic cell confiner. Starting with the made assumptions, it will continue with the equations included in the solution, then the geometrical model and FEM mesh, the solving routine and finally the different simulations that were calculated.

2.1 Assumptions

The following assumptions will be made in order to develop the stress-deformation equations :

1. Body forces, such as gravity, will not be considered, as cells are expected to experience forces much greater than their own weight.
2. Inertial forces will be neglected.
3. The materials can be defined as Neo-Hookean material, a suitable formulation for materials undergoing large deformations [17].
4. The contact between elements is frictionless.
5. The time scale of the experiment is small enough to not consider viscous effects.
6. Cells are attached to their substrate.
7. The geometrical model will be based upon the scheme presented in figure 2.

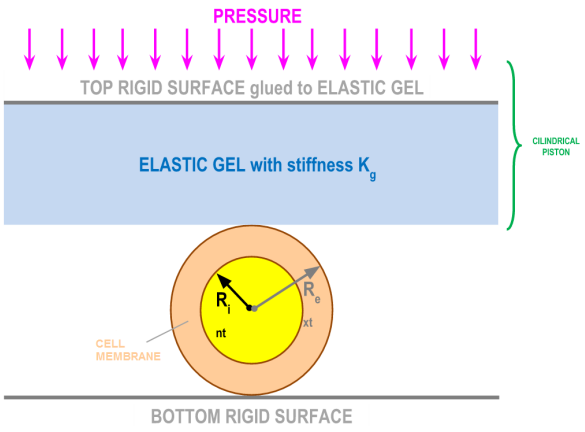

Figure 2: 2D scheme of the experiment for suspended (spherical) cells. The elements are not at scale. Reproduced with permission of its original author, Vito Conte

2.2 Equilibrium

Given a general deformable body, the Cauchy stress tensor $\boldsymbol{\sigma}$ relates the traction forces $\boldsymbol{t}$ acting over a certain point P and on a surface with normal $\boldsymbol{n}$, as:

$$\boldsymbol{t}(\boldsymbol{n}) = \boldsymbol{\sigma}\boldsymbol{n} \tag{1}$$

Stresses in the reference configuration can be expressed using the Second Piola-Kirchoff stress tensor $\boldsymbol{S}$, obtained from the Cauchy stress tensor:

$$\boldsymbol{S} = J\boldsymbol{F}^{-1}\boldsymbol{\sigma}\boldsymbol{F}^{-T^{-1}} \tag{2}$$

Where $\boldsymbol{F}$ is the rate of deformation tensor.

For a general deformable body, the local spatial equilibrium equation (equilibrium for any given point in the deformed configuration) is

$$\nabla\boldsymbol{\sigma} + \boldsymbol{f} = \boldsymbol{0} \tag{3}$$

Where $\boldsymbol{\sigma}$ represents the forces acting on the boundary, and $\boldsymbol{f}$ those acting on the volume.

According to assumption 1 equation (3) becomes

$$\nabla\boldsymbol{\sigma} = \boldsymbol{0} \tag{4}$$

2.3 Constitutive equation

Constitutive equations give the relationship between the stresses $\boldsymbol{\sigma}$ and the body's deformation. As the elastic potential Ψ represents the work done by the stresses from the initial to the current position [11], it will be used to deriver the constitutive equation of the material. For Neo-Hookean material the expression is

$$\Psi = \frac{\mu}{2}(I_c - 3) - \mu lnJ + \frac{\lambda}{2}(lnJ)^2 \tag{5}$$

Where λ and μ are the material's Lamé first and second parameters respectively, and J is the jacobian of the deformation gradient tensor.

The relationship between this elastic potential and the second Piola-Kirchoff stress tensor $\boldsymbol{S}$ is given by

$$\boldsymbol{S} = 2\frac{\partial\Psi}{\partial\boldsymbol{C}} = \mu(\boldsymbol{I} - \boldsymbol{C}^{-1}) + \lambda(lnJ)\boldsymbol{C}^{-1} \tag{6}$$

Using equation (2) to substitute $\boldsymbol{S}$ for $\boldsymbol{\sigma}$

$$\boldsymbol{\sigma} = \frac{\mu}{J}(\boldsymbol{F}\boldsymbol{F}^{\mathrm{T}} - \boldsymbol{I}) + \frac{\lambda}{J}(lnJ)\boldsymbol{I} \tag{7}$$

This equation will be included in (4)

$$\nabla\boldsymbol{\sigma} = \nabla[\frac{\mu}{J}(\boldsymbol{F}\boldsymbol{F}^{\mathrm{T}} - \boldsymbol{I}) + \frac{\lambda}{J}(lnJ)\boldsymbol{I}] = 0 \tag{8}$$

2.3.1 Analytical solution for 1D confined gel

In order to illustrate the previously shown equations, a simple version of the problem can be solved. The next assumptions will be made.

- The gel only deforms along the Z axis
- The displacement is known for the lowest (z=0, $u_0 = 0$) and highest (z=H, u_H = -d) layers

Derivation of the Cauchy stress As we are not considering the Poisson effect, the displacement field and the deformation gradient tensor will have the following expressions:

$$\mathbf{x} = \mathbf{X} + \begin{pmatrix} 0 \\ 0 \\ u_z \end{pmatrix}; \ \mathbf{F} = \frac{\partial \mathbf{x}}{\partial \mathbf{X}} = \begin{bmatrix} 1 & 0 & 0 \\ 0 & 1 & 0 \\ 0 & 0 & 1 + u'_z \end{bmatrix} \tag{9}$$

This allows us to define J and $\boldsymbol{C}$:

$$J = det(\mathbf{F}) = 1 + u'_z; \ \mathbf{C} = \mathbf{F^t F} = \begin{bmatrix} 1 & 0 & 0 \\ 0 & 1 & 0 \\ 0 & 0 & (1 + u'_z)^2 \end{bmatrix} \tag{10}$$

Being $u_z(z)$ an unknown function and u'_z its first partial derivative with respect to Z.

Considering again equation 6 and combining it with (10) we can obtain $\mathbf{S}$:

$$\boldsymbol{S} = \mu \begin{bmatrix} 0 & 0 & 0 \\ 0 & 0 & 0 \\ 0 & 0 & 1 - (1 + u'_z)^{-2} \end{bmatrix} + \lambda ln J \begin{bmatrix} 1 & 0 & 0 \\ 0 & 1 & 0 \\ 0 & 0 & (1 + u'_z)^{-2} \end{bmatrix} =$$

$$= \begin{bmatrix} \lambda ln J & 0 & 0 \\ 0 & \lambda ln J & 0 \\ 0 & 0 & \mu[1 - (1 + u'_z)^{-2}] + \lambda ln J (1 + u'_z)^{-2} \end{bmatrix}$$

And with (2):

$$\boldsymbol{\sigma} = (1 + u'_z)^{-1} \begin{bmatrix} \lambda ln J & 0 & 0 \\ 0 & \lambda ln J & 0 \\ 0 & 0 & (1 + u'_z)^2 [\mu[1 - (1 + u'_z)^{-2}] + \lambda ln J (1 + u'_z)^{-2}] \end{bmatrix}$$

And the stresses in the XY plane:

$$S_{zz} = \mu[1 - (1 + u'_z)^{-2}] + \lambda ln J (1 + u'_z)^{-2}$$
$$\sigma_{zz} = (1 + u'_z)[\mu[1 - (1 + u'_z)^{-2}] + \lambda ln J (1 + u'_z)^{-2}]$$

Displacement function u_z (z) To find $u_z(z)$, we'll apply the next conditions: Cauchy's principle for $\nabla\boldsymbol{\sigma}$, and known displacements for $u_z(z)$:

$$\begin{cases} \nabla\boldsymbol{\sigma} = 0 \\ u_0 = 0 \\ u_H = -d \end{cases} \tag{11}$$

Applying the first condition, the following equation is obtained:

$$\begin{aligned} \frac{\partial\ \sigma_{zz}}{\partial z} &= \frac{\partial(1+u'_z)^2[\mu(1-\frac{1}{(1+u'_z)^2})+\lambda\frac{lnJ}{(1+u'_z)^2}]}{\partial z} = \\ &= \mu u''_z + \mu\frac{u''_z}{(1+u'_z)^2} + \lambda\frac{u''_z(1-ln(1+u'_z))}{(1+u'_z)^2} = \\ &= u''_z[\mu(1+\frac{1}{(1+u'_z)^2}+\lambda\frac{(1-ln(1+u'_z))}{(1+u'_z)^2}] = 0 \end{aligned}$$

Therefore, the problem presents two possible solutions, either $u''_z(z) = 0$, or $\mu(1+\frac{1}{(1+u'_z)^2}+\lambda\frac{(1-ln(1+u'_z))}{(1+u'_z)^2}) = 0$

First solution: Integrating $u''_z = 0$ with respect to Z we obtain a linear $u_z(z)$:

$$u_z(z) = Az + B$$

Where A and B two constants. Applying the second and third conditions:

$$\begin{aligned} u_0 = A\cdot 0 + B = 0 \Rightarrow B = 0 \\ u_H = A\cdot H = -d \Rightarrow A = -\frac{d}{H} \end{aligned}$$

The displacement function u_z is found. As it will be later shown, this is the only possible solution.

$$u_z(z) = -\frac{d}{H}z$$

Second solution: The equation $\mu(1+\frac{1}{(1+u'_z)^2}+\lambda\frac{(1-ln(1+u'_z))}{(1+u'_z)^2}] = 0$ is an equation of the form $F(y) = 0$, where y is u'_z. Its solution is u'$_z$ = constant, and then, u_z is a linear function.

Multiplying by $(1+u'_z)^2$ and dividing by μ the equation adquires the next expression:

$$(1+u'_z)^2 + 1 + \frac{\lambda}{\mu}[1-ln(1+u'_z)] = 0 \tag{12}$$

Expressing μ and λ in terms of the material's Young modulus E and Poisson's ratio ν in (7):

$$(1+u'_z)^2 + 1 + \frac{2\nu}{1-2\nu}[1-ln(1+u'_z)] = 0 \tag{13}$$

Figure 3 shows the plot of the function for $\nu = 0$. As it can be seen, there is no solution for $\mathrm{F(u'_z)} = (1 + u'_z)^2 + 1 + \frac{2\nu}{1-2\nu}[1 - ln(1 + u'_z)]$. Increasing ν until its limit value of 0.5 does not change this fact.

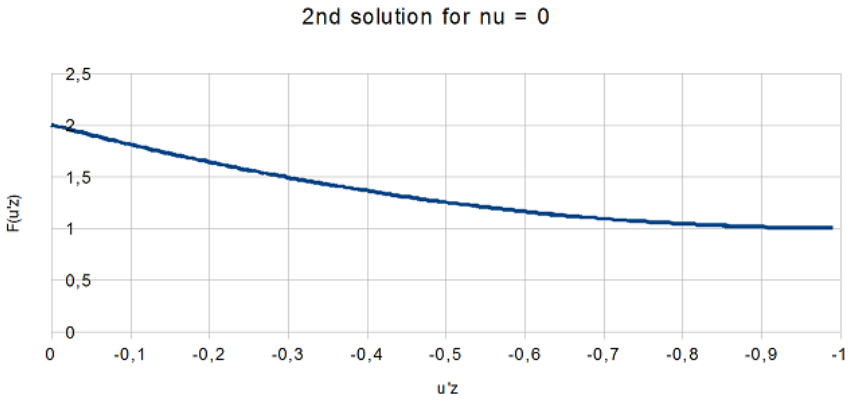

Figure 3: Analytical solution of equation (13)

2.4 Derivation of weak form

The equilibrium equations shown in the previous section are in their strong form. The next step is to express them in their weak (or integral) form, in such a way that we can extend the equilibrium to the whole body. To do so, the principle of virtual work will be applied .

Consider the equilibrium equation in (8). Premultiplying it for a virtual velocity $\delta\boldsymbol{v}$ we obtain the infinitesimal virtual work:

$$\delta\boldsymbol{w} = \nabla\boldsymbol{\sigma} \cdot \delta\boldsymbol{v} = 0 \tag{14}$$

Integrating with respect to the total volume:

$$\delta\boldsymbol{W} = \int_V \delta\boldsymbol{v} \cdot \nabla\boldsymbol{\sigma}\ dV = 0 \tag{15}$$

To open $\nabla\boldsymbol{\sigma} \cdot \delta\boldsymbol{v}$ and given that $\boldsymbol{\sigma}$ is a symmetric tensor $\boldsymbol{\sigma}^{\mathrm{T}} = \boldsymbol{\sigma}$ we apply the next relation for any second order tensor $\boldsymbol{S}$ and any vector $\boldsymbol{v}$:

$$\nabla(\boldsymbol{S}^{\mathrm{T}} \cdot \boldsymbol{v}) = \boldsymbol{S} : \nabla\boldsymbol{v} + \boldsymbol{v} \cdot \nabla\boldsymbol{S} \tag{16}$$

Substituting $\boldsymbol{S}$ per $\boldsymbol{\sigma}$ and $\boldsymbol{v}$ per $\delta\boldsymbol{v}$, and reordering (16), the total work of (15) becomes

$$\delta\boldsymbol{W} = \int_V \nabla(\boldsymbol{\sigma} \cdot \delta\boldsymbol{v}) - \boldsymbol{\sigma} : \nabla\delta\boldsymbol{v}\ dV = 0 \tag{17}$$

Applying Gauss theorem we can separate both terms of (17) into one surface integral and one volume integral:

$$\delta \boldsymbol{W} = \int_S \delta \boldsymbol{v} \cdot \boldsymbol{\sigma} \cdot \boldsymbol{n} \; dS - \int_V \boldsymbol{\sigma} : \nabla \delta \boldsymbol{v} \; dV = 0 \tag{18}$$

Reordering again, we obtain the next expression of the weak form

$$\delta \boldsymbol{W} = \int_S \boldsymbol{n} \cdot \boldsymbol{\sigma} \cdot \delta \boldsymbol{v} \; dS - \int_V \nabla \delta \; \boldsymbol{v} : \boldsymbol{\sigma} \; dV \; = 0 \tag{19}$$

We can express the gradient of the virtual velocity $\nabla \delta \boldsymbol{v}$ as the symmetric virtual rate of deformation $\delta \boldsymbol{d}$

$$\delta \boldsymbol{W} = \int_S \boldsymbol{n} \cdot \boldsymbol{\sigma} \cdot \delta \boldsymbol{v} \; dS - \int_V \delta \; \boldsymbol{d} : \boldsymbol{\sigma} \; dV \; = 0 \tag{20}$$

2.5 Finite Element Discretisation

The last step to obtain a system of equations that can be solved is the discretization of the solids into finite elements.

Considering $\boldsymbol{N_i}$, bilinear interpolation functions acting on any node i:

$$\delta \boldsymbol{v} = N_i(\boldsymbol{\xi}) \delta \boldsymbol{v_i} \tag{21}$$

Combining (21) with the following relation $\delta \boldsymbol{d} : \boldsymbol{\sigma} = \{\delta \boldsymbol{d}\}^T : \{\boldsymbol{\sigma}\}$, we can obtain:

$$\{\boldsymbol{d}\} = \boldsymbol{B}_a \delta \boldsymbol{v}_a \tag{22}$$

Where the tensor $\boldsymbol{B}_a$ is defined as:

$$\boldsymbol{B}_a = \begin{bmatrix} \partial_x N_a & 0 & 0 \\ 0 & \partial_y N_a & 0 \\ 0 & 0 & \partial_z N_a \\ \partial_x N_a & \partial_y N_a & 0 \\ \partial_x N_a & 0 & \partial_z N_a \\ 0 & \partial_y N_a & \partial_z N_a \end{bmatrix} \tag{23}$$

We use this expression to build the final system of equations, considering the nodal contributions A for every term. This way, the expression of (20) becomes:

$$\boldsymbol{g} = \mathrm{A} \; \boldsymbol{g}_a = \; \mathrm{A} \int_V \boldsymbol{B}_a^T \{\boldsymbol{\sigma}\} \; dV \tag{24}$$

This is the basic system of equations that will be solved using Newton-Raphson method to find the deformed configuration and stresses in our problem.

2.6 Contact

Having a look at the experiment in the previous chapter, the studied cells are located between two different materials, the gel above it and the glass under it. As the experiment is carried out, the gel will envelop the cell, compressing it by direct contact. In order to model the interactions between elements, several methods have been developed. For the problem presented in this document, the considered method is the Master-slave. This approach is quite different from the traditional such as the Penalty method or the Augmented Lagrangian method. To illustrate the difference and show the master slave method, they will be briefly explained and compared.

Contact overview

The general idea is the modelling of the contact through a elastic-potential (or energy)-like function representing the constraints associated to contact between bodies (usually, impenetrability). Once contact is detected, the function penalises those configurations who violate the considered constraints, increasing the total elastic potential. Usually, this means that those solutions in which one body penetrates the other will get discarded, as they imply the appearance of high forces and the increase of the total energy.

A formulation of the extended elastic potential can be seen in its unconstrained form as:

$$min\ (\delta \boldsymbol{W} + \int_{\Gamma} f(\boldsymbol{X}, q)\ d\Gamma\ ) \tag{25}$$

Where $f(\boldsymbol{X}, q)$ is the penalty function involving contact. It can be observed that the added term depends on the final configuration ($\boldsymbol{X}$) and other parameters that may be taken into consideration (q).

In order for the contact to be detected, the slave nodes coordinates are parametrised with respect to the master's surface. Consider in general two bodies, master and slave. To evaluate if there is contact the coordinates of the slave's nodes are projected into the master's surface through a mapping function. For every node i, this takes the following expression:

$$\boldsymbol{x}_{\xi_i} = \boldsymbol{\varphi}(\xi_i) \tag{26}$$

Where ξ_i is the parametrized coordinate of the node i at the master's surface, and $\boldsymbol{\varphi}(\xi_i)$ is the mapping function that projects the slave nodes into the master's surface. As contact happens at the boundary (surface for 3D bodies, and lines for 2D bodies), this projection of the slave coordinates has 1 degree of freedom less than the nodes coordinates. If we consider the normal distance between nodes:

$$\Phi(\boldsymbol{x_i}) = (\boldsymbol{x}_i - \boldsymbol{x}\xi_i) \cdot \boldsymbol{n}_{\xi_i} \tag{27}$$

$\boldsymbol{n}_{\xi_i}$ is the normal distance in the master's surface evaluated at point $\boldsymbol{x_i}(\xi)$. When $\Phi(\boldsymbol{x_i}) \leq 0$, contact is detected between node i and the master's surface.

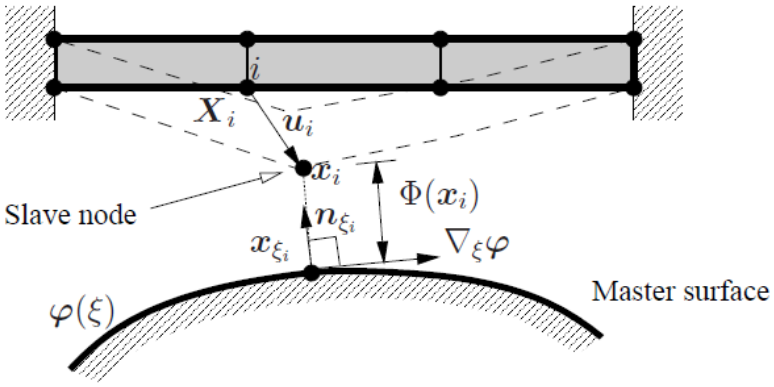

Figure 4: Scheme of the elements involved in the contact evaluation. Adapted from J. J. Muñoz [14]

2.6.1 The penalty method

The penalty method gets its name due to the inclusion of a penalty parameter p in its formulation. The contact function is

$$f(d_N, p) = \frac{p}{2}\langle -d_N \rangle^2 \tag{28}$$

Where d_N is the normal distance between nodes in contact, and $\langle -d_N \rangle^2$ makes use of the Macaulay bracket, meaning that $\langle -d_N \rangle = -d_N$ for $dN \geq 0$, and $\langle -d_N \rangle = 0$ otherwise. This way, if there is no contact between nodes ($d_N > 0$), the total energy function does not get altered. This function, although simple, has a disadvantage given by its non-differentiability in $d_N = 0$. Given that the final solution will be computed through the use of Newton-Raphson method, this fact could lead to convergence problems.

It can be inferred from (28) that the accuracy of the solution is penalty-parameter dependent. If there is contact between nodes and p is set very high, the optimal solution would be that one with close to zero distances, as d_N would have to become very low to minimize its contribution to the total elastic energy of the problem. From this point of view, and being the penalty parameter of arbitrary value, it seems like the best solution is the highest possible. But increasing its value worsens the condition number of the stiffness matrix of our problem, losing accuracy due to convergence problems. If, on the contrary, the chosen value is very low to ensure convergence, we could find solutions that imply some penetration between objects, as the added potential would not be high enough to discard such solution. An in-between value of p must then be found.

2.6.2 The augmented Lagrangian method

The Augmented Lagrangian method was developed to overcome the problems found with the penalty parameter method. In this case, contact is modelled extending the Lagrangian of the elastic potential to include some new multipliers. The energy function included is

$$f(d_N p, \lambda_N) = \frac{1}{2p}\langle -(\lambda_N + p d_N)\rangle^2 \tag{29}$$

Deriving (29) with respect to d_N we can obtain the values of the traction in the contact points:

$$t_N = -\langle -(\lambda_N + p d_N)\rangle \tag{30}$$

In order to obtain the λ_N that leads to the optimal solution, its first approximation is $\lambda_N = 0$. This yields an approximate solution and thus, an approximation of $\mathrm{t_N}$ that can be used to compute a new value of λ_N. Iterating this way (augmenting the Lagrangian λ_N) the optimal solution is found.

In comparison with the penalty method, this approach shows two important advantages: The solution converges towards the optimal solution, so p can be chosen smaller. Also, increasing the value of p between iterations speeds the process, obtaining super-linear convergence. The drawbacks of this methods are, in first place, the increase in the number of variables and degrees of freedom of the problem and its subsequent slowing; and in second place, there use of a non-differentially function (the Macaulay bracket) that can lead to convergence problems when the Newton-Raphson method is used.

2.6.3 Master-slave method

The Master-slave method, has been developed to transform the contact constrained problem into one unconstrained problem. Although at first the problem is expressed like in the augmented Lagrangian method, using a projection method known as "null-space method" the Lagrangian computations are avoided, creating instead a projection matrix that uses the parametrization of the slave nodes $\boldsymbol{N}(\boldsymbol{\varphi}(\xi))$ Taking into account some of its properties, the solution is given by the following system of non-linear equations:

$$\boldsymbol{N}^{\mathrm{T}}(\boldsymbol{\varphi}(\xi)) \cdot \nabla\Psi(\boldsymbol{x}) = 0 \tag{31}$$

For the null-space method to work efficiently, the master's surface must be smooth enough to ensure C1 and G1 continuity. This is achieved with the use of cubic B-Splines for those nodes that can be in contact, as the traditional interpolating functions do not provide these requirements. For simplicity reasons, the cubic B-Splines interpolation is usually extended to the whole master's body.

After solving (31) with Newton-Raphson method, the final configuration for every node is found. The advantages of this method in comparison with the augmented Lagrangian method are several. Firstly, there is no need to

compute Lagrangian multipliers. Secondly, the parametrization of the slave nodes is included in the operator $\boldsymbol{N}$, reducing the number of degrees of freedom of the final system of equations. Finally, in the actual computation of (31), the solutions are calculated for those nodes in contact, reducing the number of equations.

However, these advantages have a cost. A C1, G1 interpolation function must be taking into account for the master's nodes, and the original Lagrangian problem must be modified to obtain the final system of equations, adding an extra step to the process.

2.7 Incompressibility

Rubber-like materials are normally considered incompressible. Although it could have been included in the definition of the strain energy density function Ψ using a Neo-Hookean incompressible material, for instance, the solver used in the simulations is configured to work with compressible materials, adding an incompressibility routine when required. This approach also allows the model to consider incompressibility for selected areas instead of the whole body. The method used in our solution is the already explained penalty method. The expression of the functional to be minimised is adapted from V. Conte, J.J. Muñoz and M. Miodownik [15], who considered an extra term involving internal pressure. In this case is

$$\delta \boldsymbol{w} + \frac{p}{2}(V – V_0)^2 \tag{32}$$

With V the current volume and V_0 the initial volume. This way, if the penalty parameter p is set sufficiently high, the final value of V will have to be very close to the original volume V_0. To compute the volume at each iteration, the divergence theorem is applied:

$$V = \int_V dV = \int_V \frac{1}{3}\nabla(\boldsymbol{r})\, dv = \frac{1}{3}\int_S \boldsymbol{r}\cdot\boldsymbol{n}\, dS \tag{33}$$

With $\boldsymbol{r}$ the position vector for boundary S, and $\boldsymbol{n}$ the normal vector of the volume boundary.

2.8 2D model

The FEM geometry and mesh of the experiment was built using GiD software (10). According to its web page, GiD is "a universal, adaptive and user-friendly pre and post processor for numerical simulations in science and engineering". It allows to define the geometry of the model, and generate its mesh. Coupling the GiD model with a particular problem type, the different materials and conditions can be introduced to generate the final file that the solver needs.

2.8.1 Geometry

The model was built aiming to simulate the experimental setup over one single cell, instead of the whole culture. Considering every solid as homogeneous, cylindrical symmetry can be applied and work with a 2D problem. The elements included are the cell, the gel slide and the glass slide. As the size of the model can be modified later, every dimension is related to the cell's diameters. A general view on the model final geometry can be observed in figure 5, representing the meshed model. It can be observed that the relative size of the modelled gel with respect to the cell is huge. In the real experiment, the gel is around 100 times higher and 1 million times wider than cells. In our geometry, the gel is big enough to reproduce the effects of an infinite gel, but small enough to be efficiently modelled.

- The attached cell is modelled like a solid semicircle of 1 unit of diameter.
- The gel is model as rectangle of 100 units wide per 39 units high.
- The glass slide was represented as a rigid line with 120 units of length.

2.8.2 Mesh

The geometrical model was meshed with quadratic 9 node quadrilaterals, a requirement for available implementation of contact with Master-Slave. In this case, the gel was considered the master while the cell was the slave. The shape of the elements are quadrilaterals for the own nature of the modelled, as triangular elements can give problem in terms of non-deformability. Because there were no apparent restrictions in terms of mesh size, it was meshed with a fine discretisation. Figure 5 shows the final mesh, along with some information about its size. Figure 6 shows a close up of the meshed cell, as the model size makes it impossible to see the cell in detail in the previously commented figure.

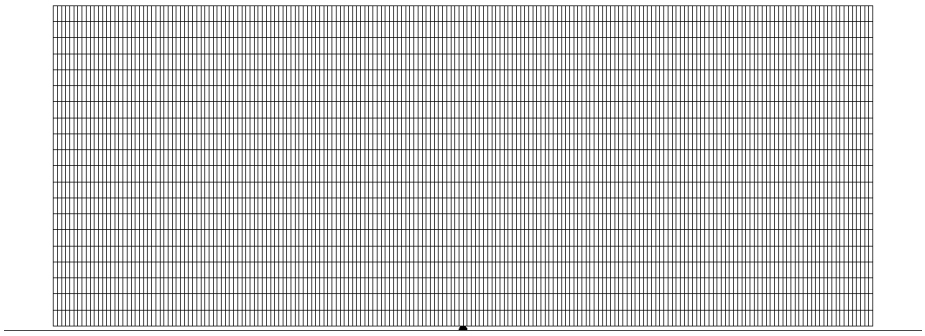

Figure 5: Meshed 2d model. The final model has 16615 nodes and 4151 quadratic elements. The big rectangle represents the gel, the bottom line the glass slide, and the black dots in the middle of them is the cell.

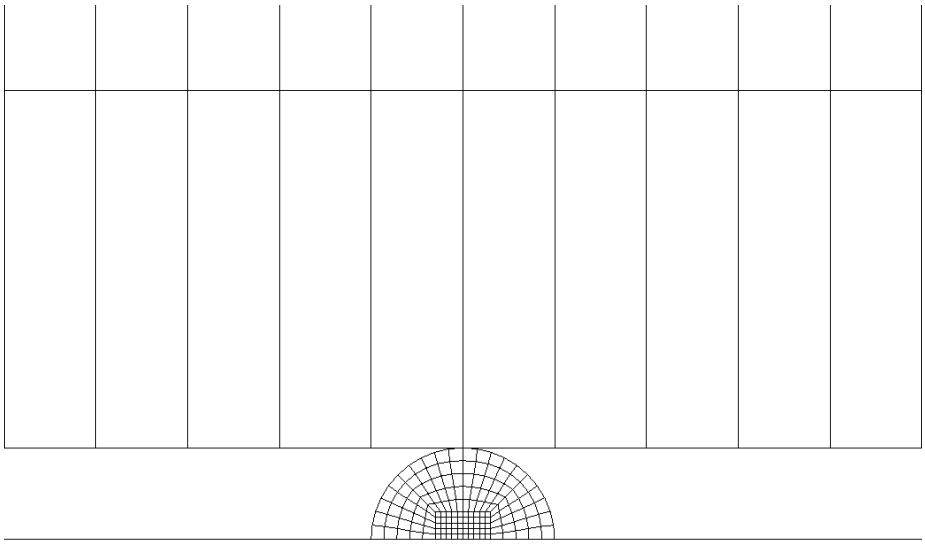

Figure 6: Closeup of meshed cell. The cell is built using 300 elements, representing only a 7.22% of the total mesh.

2.9 Simulations

2.9.1 Solver routine

The solver used in the simulations was Embryo, a FEM solver developed by UPC professor Jose Javier Muñoz, specially design for biophysical and biomechanical analysis. It was coupled with MatLab(2016b version, The Mathworks Inc) to generate an automatic iterative routine to start the computations and narrow the search for the cell's stiffness. The approach follows the bisection method used to determine roots of a function. The function (in this case the model) is evaluated at the desired points (cell's stiffness). If a root (calculated final diameter = searched final diameter) is found, the process ends. If it is between two considered points, the next search interval takes those as extreme points and starts again, evaluating the function inside the updated search interval.

The files involved in this process are the data files, and the results files. The data files contain information about the solving process (like number of steps, tolerance of the results or integration method) and information about the model (material information, nodes coordinates and connectivity matrix, constraints and conditions imposed). The result files contain the displacements and stresses per node and step.

For any gel stiffness the routine followed is the same:

1. The geometrical data of the generic model is scaled according to the initial cell's size. The gel material properties are also changed to that of the test.

2. The modified data file is copied as many times as cell's stiffness are going to be tried in this step. For each one of them, the cell's stiffness is changed according to the tested value.

3. FEM computations are performed and the final diameters are read.

    - If the final diameter is within tolerance, the search for this diameter ends

4. The search interval for cell's stiffness is updated with the values the objective diameter is in. Go back to 2

Figure 7 shows an example scheme of this process for any given diameter and gel stiffness and 3 different cell's stiffness per iteration.

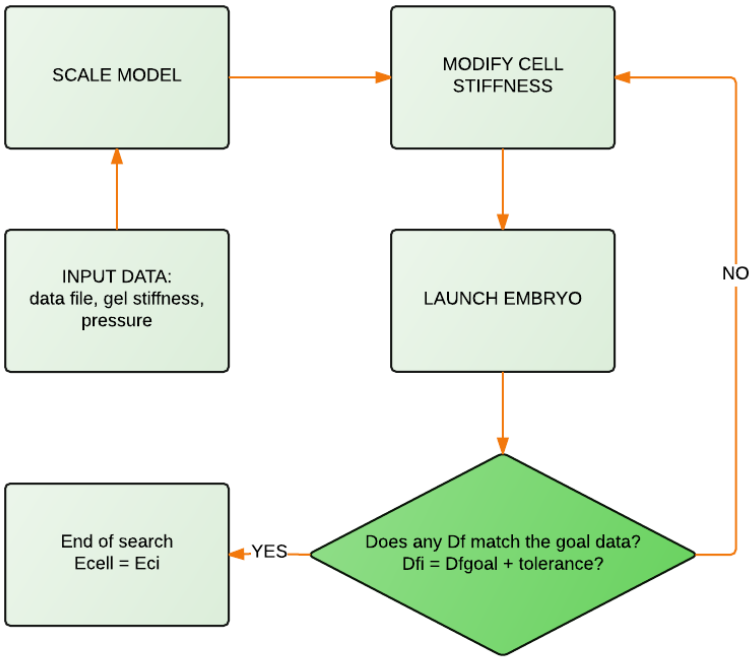

Figure 7: Flux diagram of the solver routine, set for the minimum number of cell's stiffness. In this case, we only perform 1 new analysis per iteration, for the stiffness in the middle of the updated interval [Ec1 Ec3]

2.9.2 Configuration

The model was simulated with 7 different values of gel stiffness: 1 kPa, 5 kPa, 10 kPa, 15 kPa, 20 kPa, 25 kPa and 30 kPa.

The 1 kPa simulation served as a reference to calculate the initial cell's stiffness. This value can be used to build Deformation - Gel stiffness curves for the preliminary value, and check if that stiffness remains constant. The rest of the tests supplied enough data to create a Deformation - Cell stiffness chart to provide fast estimation of the cell's stiffness. Having 6 different values of gel stiffness allows us to map the space Gel stiffness - Deformation - Cell stiffness with enough precision.

Considering the initial diameter, the expression of the deformation was done using a parameter λ, such as $D_f = \lambda D_0$. In order to provide an example of the solutions for a constant value of cell stiffness, the final diameter included in the reference simulation does not correspond to any real cell. Nevertheless, the value of the calcualted in that simulation can be used to establish the trend. For this project, it was $\lambda = 1.25$, meaning that the reference stiffness was that

one corresponding to a final diameter 25% bigger than the original. The values of λ used in the other simulations were 1.500, 1.625, 1.750, 1.875 and 2.000.

The input data left to define is the penalty parameter p and the Poisson's ratio ν. After some preliminary simulations with p ranging from 0.0001 to 1000, it was observed that results weren't particularly affected by p . For convergence reasons, it was set to 0.0001. Although the first version of the model considered $\nu = 0.3$, the cells were not able to deform as much as it was expected. The final chosen value of ν for all materials was 0.49.

3 Results

3.1 Convergence

Some tested values of cell's stiffness led to convergence problems. Nevertheless, the general trend of the results was not affected by this fact, allowing us to predict the deformation for every simulated gel.

3.2 Model behaviour

GiD postprocessor was used to check if the model behaved properly. Figure 8 shows the initial and the final configuration of the whole model. When the simulation ends, the gel surrounds and squeezes the cell under it. As we move far from the cell's position, the gel eventually touches the glass slide (the rigid line in the model). In figure 9 we can see the vertical displacement for a gel of 5 kPa under a cell of (approximately) 1.5 kPa. The area of effect of the cell is concentrated in the contact zone. As we move upwards, the influence becomes smaller. At the top layers is almost unnoticed.

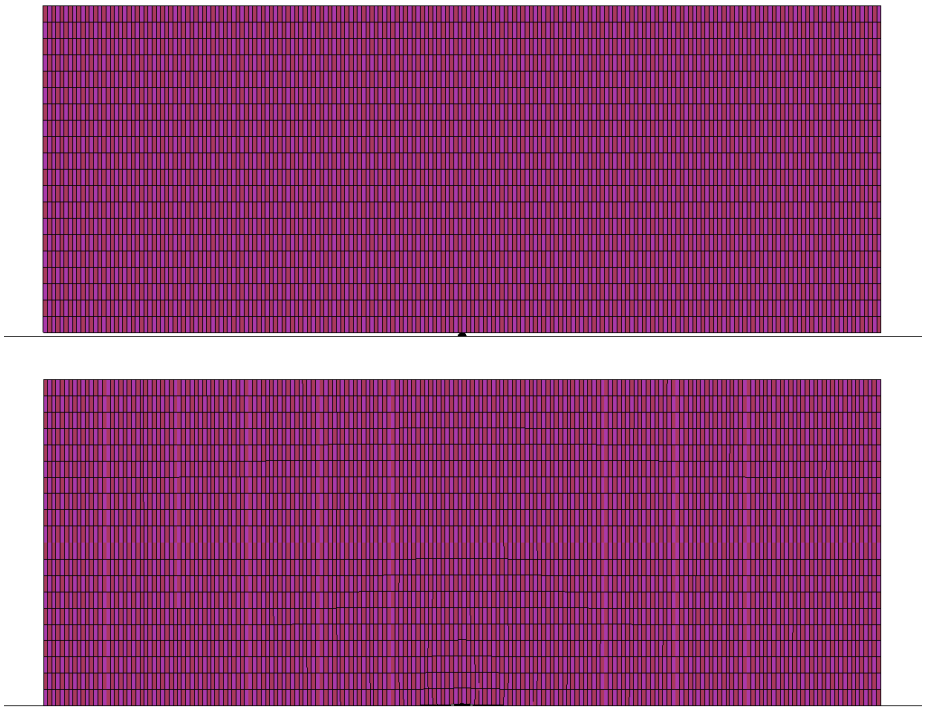

Figure 8: Comparison between initial and final configuration

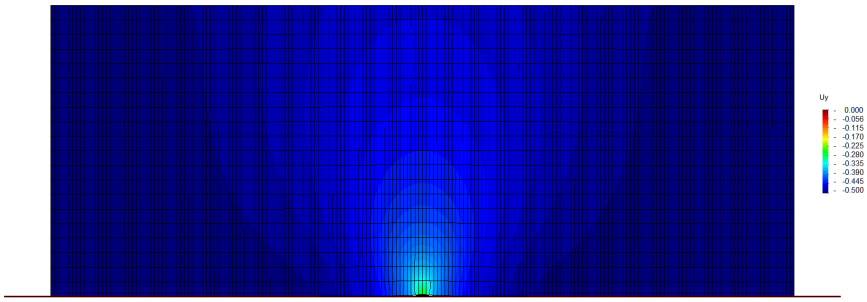

Figure 9: Vertical deformation for a gel of 5 kPa over a cell of 1.5 kPa

Figure 10 shows a close up on the cell. We can see that the gel does not cover all the external surface, leaving a gap. Eventually, and because the gel was set sufficiently wide, the gel touches the glass slide.

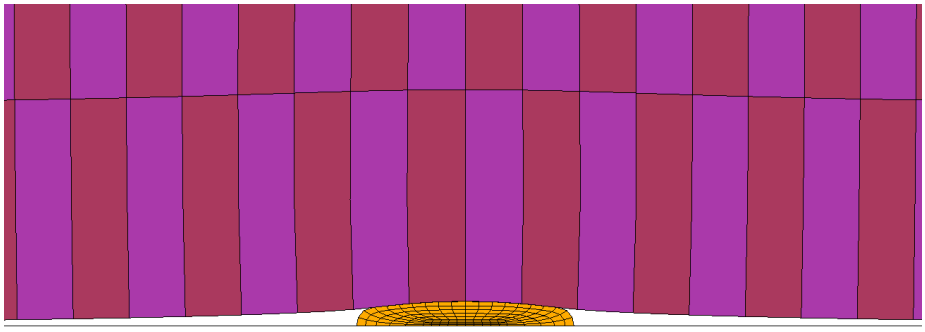

Figure 10: Close up picture of the deformed configuration

3.3 Cell final diameter vs gel stiffness

The different tests showed similar stiffness - deformation trends for every value of gel's stiffness. They can be found in figure 11. Figure 12 shows the predicted final diameters for the standard stiffness.

Figure 11 can be used as an abacus for experimentalists to find differences in the compliance between healthy cells and their diseased counterpart, such as normal and cancer cells for instance. Using the data extracted from experimenting with the dynamic cell confiner, they could easily extract an approximation of the stiffness. For example, if a 30 kPa test was performed over attached cells

and their final horizontal diameter was 80% greater than the initial one, looking at the chart would yield a value of around 2.1 kPa for its stiffness.

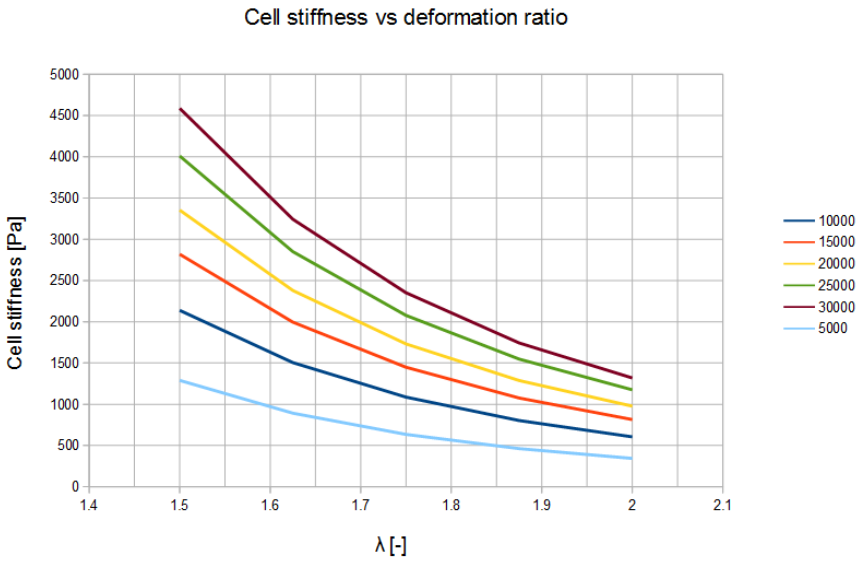

Figure 11: Relationship between cell's stiffness (Pa) and deformation (adimensional value) for every simulated gel.

It can be observed, that for a given value of cell's stiffness, the higher the stiffness of the gel, the higher the deformation of the cell. At the same time this means that in order to achieve the same deformations in cells, the cell's stiffness has to increase as the gel stiffness increases. The reason is the share of the total pressure imposed over the gel. If both gel and cell have similar stiffness, the deformation is more equally divided between them. But, as the gel becomes stiffer, it starts to behave more and more like a rigid body with respect to the cell. The cell experiences more pressure, and thus, is more deformed.

GiD allows us to observe this phenomenon in our simulations. Figure 13 provides a comparison between different gel stiffness. Looking at the results for a constant value of cell's stiffness, we can see how cells get more and more flattened in their contact surface, being more squeezed and thus achieving higher deformations.

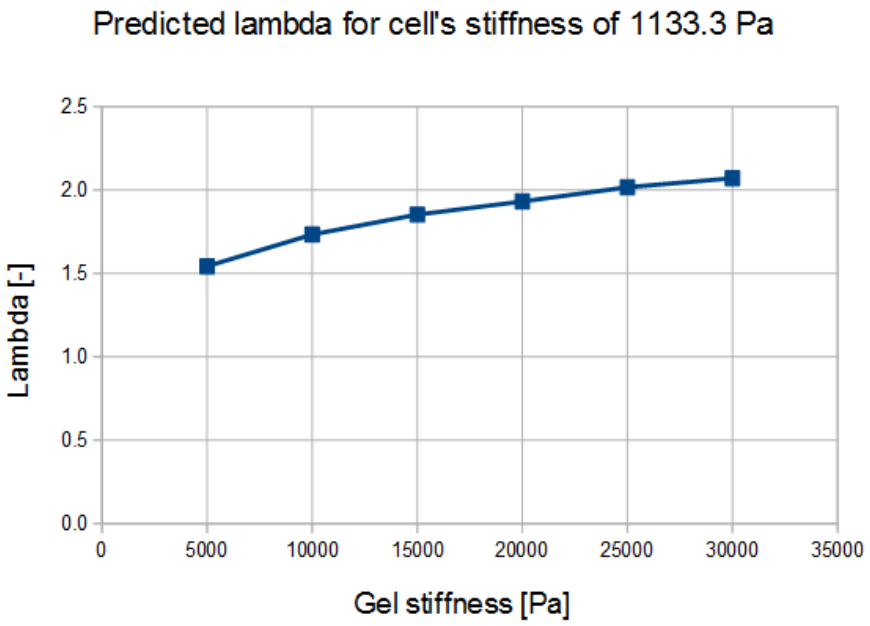

Figure 12: Prediction of cell's final diameters (adimensional values) under different gel stiffness (Pa) for a constant value of cell's stiffness. The 1133.3 Pa value was the stiffness retrieved from the reference simulation

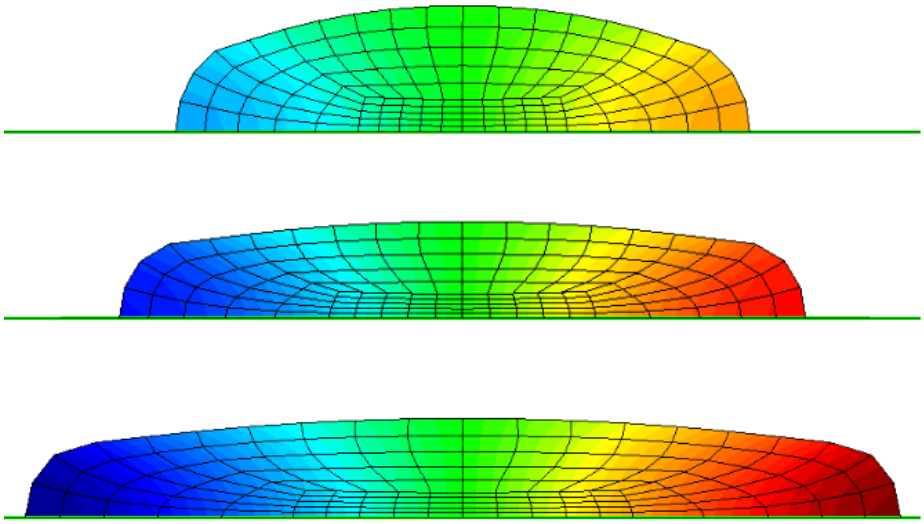

Figure 13: Deformed configuration for cells of 1.5 kPa with gels of 5, 20 and 30 kPa respectively. The colors represent the lateral displacements of the nodes. We can see how, as gel stiffness increases, cells are more deformed.

4 Discussion and further steps

4.1 Discussion

The objectives of the project were successfully achieved. The modelled cells behaved as it was expected, and the experiment could be reproduced. The results allowed us to map the Deformation - Gel stiffness - Cell stiffness space, and build charts for fast identification of cell parameters. At the same time, this charts can be used to predict the cell's response under different gel stiffness, and see if there is some change in their material parameters over time, a useful tool for disease research. If the predicted deformation is progressively underestimating the experimental data, this would mean that the cell is becoming softer as the environment (in this case, the gel) becomes stiffer. If it overestimates the experimental data, the cell is adapting itself, and hardening. From a biological point of view, this could help us to study two phenomena:

- Changes in the stiffness of cells affect their deformability. Several research have concluded that cancer cells are softer that healthy cells [1,2,4]. This softening would make it easier for them to migrate throughout the body, expanding the cancer and producing metastasis.

- In order to balance changes produced in their environment, cells would have to modify their stiffness accordingly. As cancer develops, the tissue surrounding the tumour becomes stiffer. In this direction, breast cancer cells (2) were found to adapt better than healthy cells under very stiff environments.

In conclusion, the method can be used to study the evolution of cell's parameters, as well as study the differences between different sets of cells, like cancerous and healthy cells, for instance. At the same time, once they are fully characterized with this method, it would allow researchers to classify them according to the deformation.

About the accuracy of the results, it must be said that the obtained results are as accurate as our assumptions. Discrepancies between the real stiffness and the calculated values may come from:

- The definition of the material: Although Neo-Hookean material is commonly used for modelling rubber-like materials, there are other possible choices for materials that undergo very large deformations, like Monley-Rivin or Ogden [18].

- Spatial distribution of cellular structures: The calculated stiffness is not the stiffness of cellular tissue, but the stiffness they would have if they were isotropic, homogeneous solids. They represent, under the assumed circumstances, apparent macroscopic values.

- Viscosity: The immediate response of the cell during the experiment was the basis on the elastic modelling of the cell. If the time-scale of the viscous

behavior was small enough to influence the results, a more complex model would be necessary.

4.2 Further steps

The model presented in this thesis is simple. It can be considered as a first version, and use the obtained results to improve it and develop a more complex model that reproduces better cellular mechanics. Below, is a list of proposed changes:

- Modelling of suspended cells: The only change in the current model would be the cell geometry, which would be spherical (or a complete circle, given the 2 dimensions of the model)
- Extension of model from 2D homogeneous semicircle to 3D homogeneous semi-sphere: Maintaining the assumptions of homogeneity and isotropy, the 3D model is perhaps the obvious evolution. It would also allow us to evaluate the accuracy of the 2D assumption comparing the results between both models
- Change the cell material definition to Ogden material: It was observed that the cell was very deformed at the end of the simulations. Although Neo-Hookean materials, as assumed, are generally suitable for rubber materials undergoing large deformations, the Ogden material was developed for rubber materials at even higher strains [16]. For incompressible materials [17], the strain energy density is

$$\Psi = \sum_{p=1}^{N} \frac{\mu_p}{\alpha_p} (\lambda_1^{\alpha_p} + \lambda_2^{\alpha_p} + \lambda_3^{\alpha_p} - 3) \tag{34}$$

  Where N, μ_p and α_p are material parameters. To find these values it is necessary to perform assays and fit the data through statistical analysis.

- Change of model from elastic solid to visco-elastic shell: This new model would consider the cell interior as an incompressible viscous fluid, and the actin cortex and the membrane as an elastic shell. With respect to the viscosity behaviour, the stress defined in the *Numerical Model* section should be modified to add an extra term, dependent on the rate of deformation $\boldsymbol{F}$ [12]. Also, to model it properly, it is required data about the thickness of the external layer and about the temporal evolution of cell's response, so as to define the geometry and the viscosity parameter respectively.

5 References

[1] S. Suresh, 'Biomechanics and biophysics of cancer cells', *Acta Biomater*, vol. 3, no.4, July 2007, pp. 413–438

[2] E. L. Baker et al, 'Cancer Cell Stiffness: Integrated Roles of Three-Dimensional Matrix Stiffness and Transforming Potential' *Biophysical Journal*, vol. 99, October 2010, pp. 2048–2057

[3] A. Mietke et al, 'Extracting Cell Stiffness from Real-Time Deformability Cytometry: Theory and Experiment' *Biophysical Journal*, vol. 109, November 2015, pp. 2023–2036

[4] K. Haasel and A.E. Pelling, 'Investigating cell mechanics with atomic force microscopy' *J. R. Soc.* Interface 12: 20140970.

[5] J. Phenner et al, 'Macroscopic Stiffness of Breast Tumors Predicts Metastasis', *Sci. Rep* 4, 5512

[6] N. Gavara and R. S. CHadwick, 'Relationship between cell stiffness and stress fiber amount, assessed by simultaneous atomic force microscopy and live-cell fluorescence imaging', *Biomech Model Mechanobiol*, 2016, vol. 15, pp. 511–523

[7] J. Guck et al, 'The Optical Stretcher: A Novel Laser Tool to Micromanipulate Cells', *Biophysical Journal*, August 2001, vol 81, pp. 767–784

[8] M. Le Berre et al, 'Methods for Two-Dimensional Cell Confinement', *Methods in Cell Biology*, 2014, vol 121, pp. 213-229

[9] S. E. Cross, 'Nanomechanical analysis of cells from cancer patients', *Nature Nanotechnology*, 2007,vol. 2, pp. 780 - 783

[10] A. Saha et al, 'Determining Physical Properties of the Cell Cortex', *Biophysical Journal*, March 29 2016, no. 110, pp. 1421–1429

[11] J. Bonet and R. D. Wood, 'Nonlinear Continuum Mechanics for Finite Element Analysis', *Cambridge University Press*, 2nd edition, 2008

[12] J. J Muñoz, 'Modelling of embryonic invagination: Computational aspects', April 2016

[13] G. Kloosterman, 'Contact Methods in Finite Element Simulations', University of Twente, 2002

[14] J. J. Muñoz, 'Modelling unilateral frictionless contact using the null-space method and cubic B-Spline interpolation' *Computer Methods in Applied Mechanics and Engineering*, vol. 197, Issues 9-12, 2008, pp. 979-993

[15] V. Conte, J.J. Muñoz, M. Miodownik, 'A 3D finite element model of ventral furrow invagination in the Drosophila melanogaster embryo', *Journal of the Mechanical Behavior of Biomedical Materials*, vol. 1, Issue 2, 2008, pp. 188-198

[16] R. W. Ogden, 'Large Deformation Isotropic Elasticity—On the Correlation of Theory and Experiment for Incompressible Rubberlike Solids', *Rubber Chemistry and Technology*, Vol. 46, No. 2, May 1973, pp. 398-416

[17] K. Weinberg, 'Lecture Notes for Zur Methode der finiten Elemente in der Mechanik II: Nichtlineare Probleme', TU Berlin [in English]. http://mech2.pi.tu-berlin.de/weinberg/Lehre/fem2/Chapter4.pdf

[18] R. W. Ogden,'Non-Linear Elastic Deformations', *Ellis Horwood Ltd.*, 1984